Preprint
UCRL-JC-145022

Propagation of Axially Symmetric Detonation Waves

R.L. Druce, F. Roeske, Jr., P.C. Souers, C.M. Tarver, C.T.S. Chow, R.S. Lee, E.M. McGuire, G.E. Overturf III, P.A. Vitello

This article was submitted to
12th International Detonation Symposium
San Diego, CA
August 11-16, 2002

June 26, 2002

U.S. Department of Energy

Lawrence
Livermore
National
Laboratory

Propagation of Axially Symmetric Detonation Waves*

Robert L. Druce, Franklin Roeske, Jr., P. Clark Souers, Craig M. Tarver,
Charles T. S. Chow, Ronald S. Lee, Estella M. McGuire, George E. Overturf III and Peter A. Vitello
Lawrence Livermore National Laboratory
Livermore, CA 94550

We have studied the non-ideal propagation of detonation waves in LX-10 and in the insensitive explosive *TATB*. Explosively-driven, 5.8-mm-diameter, 0.125-mm-thick aluminum flyer plates were used to initiate 38-mm-diameter, hemispherical samples of LX-10 pressed to a density of 1.86 g/cm^3 and of *TATB* at a density of 1.80 g/cm^3. The *TATB* powder was a grade called *ultrafine (UFTATB)*, having an arithmetic mean particle diameter of about 8-10 µm and a specific surface area of about 4.5 m^2/g. Using PMMA as a transducer, output pressure was measured at 5 discrete points on the booster using a Fabry-Perot velocimeter. Breakout time was measured on a line across the booster with a streak camera. Each of the experimental geometries was calculated using the Ignition and Growth Reactive Flow Model, the JWL++ Model and the Programmed Burn Model. Boosters at both ambient and cold (-20 °C and –54 °C) temperatures have been experimentally and computationally studied. A comparison of experimental and modeling results is presented.

INTRODUCTION

The properties of non-ideal explosives sometimes make them more difficult to utilize, but these same properties greatly reduce the chance of unintended reaction or detonation, both in utilization and in storage. TATB is such an explosive, having a reaction zone > 1 mm. There is an ongoing study at Lawrence Livermore National Laboratory (LLNL) of the detonation output properties of *UFTATB* boosters. The study includes boosters of various ages and powder batches. Since the ability of the detonation wave to burn uniformly throughout the main charge high explosive is one of the properties that can materially affect performance, we are monitoring parameters that will be affected by corner turning in the booster. Diagnostics include velocimetry at five discrete points and a streak camera. The positions of the velocimeter probes were chosen to provide data at several points on a line of constant longitude on the booster. The streak camera view was chosen to provide timing confirmation and to provide a link with experiments conducted previously with only streak camera diagnostics. It has been shown that anomalies in the detonation wave are accentuated at reduced temperature. For that reason, we detonated boosters at ambient temperature, -20 °C and -54 °C to study the effect of temperature as the boosters age.

THE BOOSTERS

The booster of interest is a 3.8 cm diameter hemisphere of *UFTATB* with an average density of 1.80±0.005 g/cm^3. The boosters are formed by uniaxially compacting a known mass of *UFTATB* powder (8 µm mean particle size, 4.5 m^2/g specific surface area) into a hemispherical die of known final volume. This method yields the correct bulk density for the overall booster, however localized inhomogeneities occur because of the frictional packing of the particles at the die walls and at the moving ram face. Given that the compaction forces are normal to the axis of rotation within this hemispherical part, the inhomogeneities tend to be axisymmetric, allowing a 2-D representation of the inhomogeneities. The *UFTATB* boosters were inspected using a computer aided tomography x-ray scanner. The detector for the scanner is a 14-bit 1K x 1K Apogee CCD camera lens-coupled to a Terbium activated glass scintillator. The x-ray source for the system is a PHILIPS 450 kVp tube and generator. For these small parts we made use of the 5 cm field of view (50 _m pixels size at the scintillator), and had the source parameters at 200 kVp, 4.5 mA, with the 1 mm spot. The source and object were positioned to ensure a source blur of less than a pixel at the center of the object. To improve the signal-to-noise ratio within the data set, all voxels within the same axisymmetric radius are averaged together and shown as a radial average density plot as shown in Figure 1. The highest densities are found at the ram face near the die wall. The lowest densities are found near the pole because the force cannot fully transfer through the part to

* This work was performed under the auspices of the U.S. Department of Energy by the University of California, Lawrence Livermore National Laboratory under Contract No. W-7405-Eng-48.

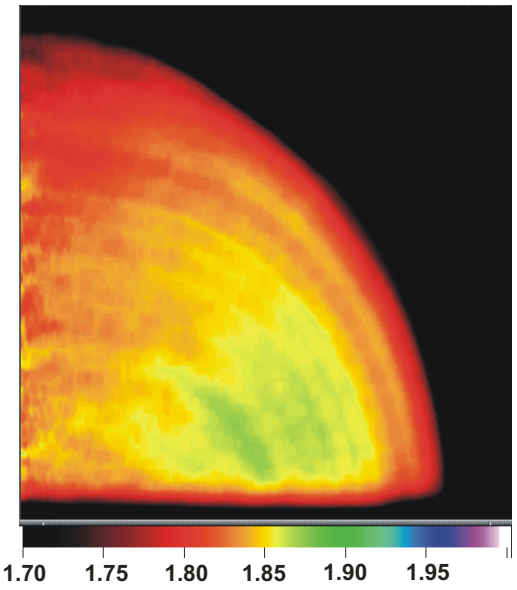

Figure 1. False-color representation of the radial average densities in a pressed booster of ultrafine TATB. Color bar represents densities in g/cm^2.

fully compact this region. Density variations within boosters are typically found to be within 2-3%.

The first set of four shots used a near-ideal explosive, LX-10 (95% HMX/5% Viton A), as a surrogate for the *UFTATB* boosters. The LX-10 surrogates were machined to a 3.8 cm diameter hemisphere from an LX-10 billet that was pressed to a density of 1.86 g/cm^3. The LX-10 surrogates were used to provide calibration with a known, near-ideal explosive. Two of the LX-10 boosters were point-initiated with hemispherical detonators. The boosters initiated by hemispherical detonators had a hemispherical cavity machined into the flat surface to place the initiation point at the center of the hemisphere.

EXPERIMENT

The two types of detonators used in the investigations were a hemispherical exploding bridge wire detonator (EBW) and a two-stage slapper detonator. The hemispherical EBW detonator has an output that is uniform in time and pressure over a hemispherical surface. In the two-stage slapper detonator, an electrical slapper initiates an LX-16 (96% PETN/4% FPC 461) pellet, which throws a second aluminum flyer 5.8 mm in diameter and 0.125-mm-thick. The aluminum flyer shock-initiates the flat surface of the booster to transfer the detonation to the booster. This detonator has a stainless steel surface in intimate contact with the entire flat surface of the booster (except for the area impacted by the aluminum flyer).

The shot assembly consists of the hemispherical booster, initiated by the EBW or two-stage slapper detonator, with a PMMA shell around the periphery of the booster. The PMMA shell forms a window and mount for PMMA plugs used as pressure transducers.

A streak camera is used to view the detonation breakout along the entire periphery of the booster from equator-to-pole-to-equator.

Fabry-Perot velocimetry is utilized to determine the detonation pressure at five discrete points along the periphery of the booster from the pole to the equator at an azimuth of 90 degrees to the plane of the breakout observations. The velocimeter utilizes Doppler-shifted light to analyze the velocity of a reflective surface. This system consists of a laser light source and an analyzer that is made up of a single Fabry-Perot interferometer and five electronic streak cameras to record the velocity records. The velocimetry probes are non-contact devices that are aimed at the surface of the booster at angles of 3^o or 7^o, 30^o, 60^o, 75^o and 85^o relative to the pole. The 3^o/7^o probe is offset from the pole to give the streak camera a clear view of the booster at the pole. The breakout observation is used to confirm timing and to provide a link to past experiments, which utilized breakout observations as the sole diagnostic. Photo 1 is a view of the experiment fixture for a cold experiment with a booster installed. A custom probe designed and manufactured on-site is used for illumination and return light collection. The diameter of the focal spot at the experiment is approximately 300 µm. There is a small section of 12.7 _m thick aluminum foil placed over the booster at each Fabry-Perot viewing location with the dull side toward the probe to provide a semi-diffuse reflector on the booster surface. The probe collects a part of the Doppler-shifted light reflected from the booster to return to the analyzer. The analyzer consists of conditioning optics, the Fabry-Perot interferometer, and streak cameras as recording media[1]. The Fabry-Perot interferometer is a Burleigh adjustable cavity model set to 4.585 cm separation with a velocity constant of 870 m/s/fringe. All streak cameras are triggered at the same time and the record lengths are set

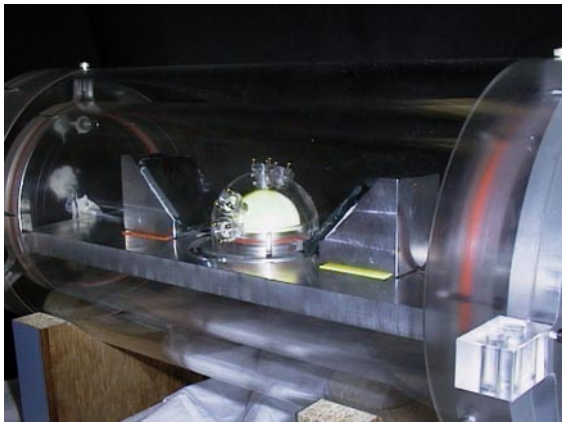

Photo 1. Photo of cold booster fixture showing booster and cooling enclosure.

according to the shot requirements. The record length varies from 1.2 to 2.4 _s for a 3 cm long sweep.

The PMMA plugs serve as pressure-transducing windows for the velocimeter. The shock wave from the detonation propagates through the aluminum foil and the PMMA with properties that are governed by the respective shock impedance of the HE and the PMMA. Since the Hugoniots of the aluminum foil and PMMA are known, it is possible to calculate the shock pressure in the PMMA. from the equations

$$P = \rho_0 U_s U_p$$

and

$$U_s = c_0 + sU_p$$

where U_s and U_p are the shock and particle velocities, respectively. ρ_0, c_0 and s are material constants that are known for PMMA[2,3]. We used a Hugoniot developed at Los Alamos National Laboratory[4]. The form is

$$U_p < 0.5 mm/\mu s$$
$$U_s = 2.774 + 2.182U_p + 2.014U_p^2$$
$$U_p > 0.5 mm/\mu s$$
$$U_s = 2.57 + 1.54U_p .$$

There is a small correction to the particle velocity due to strain-induced refractive index changes in the PMMA by the shock wave propagating ahead of the reflective surface. This correction is less than 2% for PMMA and is ignored. There is also a correction as the diverging shock wave propagates in the PMMA. This correction is small initially and grows in magnitude as the shock wave outruns the reflective surface. Since we are primarily interested in the early-time propagation, this correction is also ignored. The PMMA used was pre-shrunk and conformed to Military Specification L-P-391D. Knowing this information allows us to calculate the shock pressure from the observed velocities and the known material constants. We will describe later in the paper how these experiments provided a unique opportunity to test the PMMA Hugoniot.

The streak camera viewing the detonation breakout is a Cordin model 132 rotating mirror camera set to 5000 RPS. This setting gives approximately 20 mm/_s on the film with a total record length of 15 _s.

MODELS

Ignition and Growth (I & G) Model

The Ignition and Growth reactive flow model of shock initiation and detonation of solid explosives has been incorporated into several hydrodynamic computer codes and used to solve many 1D, 2D, and 3D explosive and propellant safety and performance problems[6-12]. The model uses two Jones-Wilkins-Lee (JWL) equations of state, one for the unreacted explosive and one for its reaction products. Both equations have the same temperature dependent form:

$$p = Ae^{-R_1 V} + Be^{-R_2 V} + \frac{\omega C_V T}{V} \qquad (1)$$

where p is pressure in Megabars, V is relative volume, T is temperature, ω is Gruneisen coefficient, C_V is average heat capacity, and A, B, R_1, and R_2 are constants. The reaction rate law for the conversion of explosive to products is:

$$\frac{dF}{dt} = I(1-F)^b(\rho/\rho_o - 1 - a)^x \quad (0 < F < F_{G_2 \min})$$

$$+ G_1(1-F)^c F^d p^y \quad (0 < F < F_{G_1 \max})$$

$$+ G_2(1-F)^e F^g p^z \quad (F_{G_2 \min} < F < 1) \qquad (2)$$

where F is the fraction reacted, t is time, ρ is the time-varying density, ρ_o is the initial density, and I, G_1, G_2, a, b, c, d, e, g, x, y, and z are constants. The mixture equations for the Ignition and Growth assume pressure and temperature equilibration between the unreacted explosive and the reaction products. The pressure equilibration constraint is an absolute necessity at the extreme pressures reached in reacting solid explosives. The temperature equilibration assumption applies in the high pressure, high temperature, turbulent mixing reactive flows produced by shock initiation and detonation. Sufficient zoning must always be used to ensure that the calculations are converged.

This three term rate law models the three stages of reaction generally observed in shock initiation and detonation of heterogeneous solid explosives. The first term represents the ignition of the explosive as it is compressed by a shock wave creating heated areas (hot spots) as the voids in the material collapse. The fraction of explosive ignited by a strong shock wave is approximately equal to the original void volume[6]. For shock initiation, the second term in Eq. (2) models the growth of reaction from the hot spots into the surrounding solid as a deflagration-type process of inward and/or outward grain burning. The exponents on the (1 - F) factors in the first two terms of Eq. (2) are set equal to _ to represent the surface to volume ratio for spherical particles. The third term in Eq. (2) describes the rapid transition to detonation observed when the growing hot spots begin to coalesce and transfer large amounts of heat to the remaining unreacted explosive particles causing them to react very rapidly. For detonation, the first term still ignites a few percent of the unreacted explosive just behind the shock front, which compresses the explosive to the von Neumann spike state. The second reaction models the rapid formation of the major reaction product gases (CO_2, N_2, H_2O, CO, etc.). The third term is used to describe the relatively slow diffusion controlled formation of the solid carbon particles in the form of diamond, graphite, or amorphous carbon. For HMX-based explosives, the last 10% of the chemical energy release is assumed to be carbon formation, while, for TATB-based explosives, the last 20% of the energy release is assumed to be solid carbon formation.

The I & G model has been incorporated into several computer codes. Results from two implementations of the I & G model applied to the hemispherical booster problem will be presented here. One implementation will be referred to as the I & G DYNA2D model and the other will be referred to as JWL++ model throughout the remainder of this paper. The I & G DYNA2D model is described in a companion paper at this symposium[5]. The JWL++ model is described below.

I & G JWL++ Model

JWL++ is a simplified version of Ignition & Growth, designed to represent detonation only[14]. It consists of an unreacted Murnaghan EOS, a reacted P-V JWL, a pressure mixer and the rate equation. Temperature and energy do not enter explicitly into the model, which is driven solely by pressure and volume. The mixer is a simple algebraic "partial pressure" term, which has been shown to be as accurate as the pressure equilibrator for LX-17 problems at 4 zones/mm. The rate term runs off P + Q, the sum of pressure and artificial viscosity, rather than just pressure, which allows minimum changes with coarse zoning. The simplicity of the model allows it to be set up, using CHEETAH and size effect data, on a new explosive in about an hour. The detonation rate in JWL++ creates the size effect, detonation front curvature and reduced velocities in turns, and, despite its simplicity, the model is able to fit most kinetic detonation data. The rate constant in the code, G_1, may be approximated by using the CHEETAH C-J pressure and the slope of the unconfined size effect curve[15].

$$\left[G_1(\text{code})\right] \approx \frac{1}{P_{cj}^{b1}} \frac{-DU_S}{\frac{\partial U_S}{\partial(1/R_O)}} \qquad (3)$$

JWL++ runs in a 2-D ALE code with CALE-like characteristics. For this problem, we used a reduced-connectivity mesh. The zoning was

rectangular in the section to the left of the explosives, ie. in the PETN, the gap and the metal, and also in the almost-square section of explosive at the top right from which the 60° arrow comes. The outer explosive zones are radial, so that a square-to-radial transition takes place at the edge of square. The zoning in the rectangular sections was almost square at about 7 zones/mm. The radial zoning was 1 degree so that the zones elongated near the outer surface. The short zone edge was 3.5 zones/mm, which is still at the edge of convergence for LX-17. This is the coarsest zoning that puts about 4 zones in the explosive's reaction zone and allows Reactive Flow to operate without greatly distorted input coefficients. Most of the zoning is well within the edge of convergence.

RESULTS

Table I shows a matrix of experiments conducted to date. The LX-10 experiments will be described first. Two of the LX-10 events were initiated with a hemispherical detonator and two were initiated with a two-stage slapper detonator. Several records were lost during the LX-10 series of experiments. This loss was attributed to problems with the fit of the PMMA shell over the HE. Tolerances of 12.7 _m over the entire hemispherical surface were required to ensure proper fit. To address the tolerance problem in later experiments, plugs were placed at strategic points on the PMMA shell to provide a good fit between the PMMA and the HE. The plugs are visible in Photo 1. The plugs eliminated gaps and eliminated lost records in ambient shots. Shots at reduced temperature still show lost records, however. This phenomenon is still under investigation. Figure 2 shows a typical raw Fabry-Perot record taken on the LX-10 experiments. Note from Fig. 2 that there are additional fringes that can be attributed to a reflection from the shock, allowing observation of the shock velocity directly.

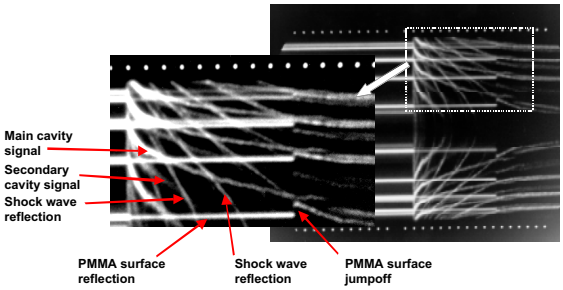

Figure 2. Raw Fabry-Perot record showing the various fringe positions and their interpretation. This record is very information-rich, but difficult to analyze.

Direct observation of the shock velocity affords an opportunity to check the validity of assumed material properties. A comparison of the observed shock and particle velocities with the Hugoniot relations published by Los Alamos National Laboratory[4] gives excellent agreement (better than 5%), indicating that our material is very similar to the Los Alamos reference material. Figure 3 is a comparison of particle velocity and pressure histories for the aluminum foil at the *UFTATB*/PMMA interface for a typical LX-10 shot. The peak velocity is about 3.17 km/s with a peak pressure of approximately 281 kbar for the experimental results with the I & G DYNA2D model indicating about 3.0 km/s velocity and 256 kbar pressure. The indicated velocity and

Table I. Matrix of experiments conducted to date.

HE type	Detonator	HE batch	Pressing year	Temp.	Case number	No. of shots
LX-10	Hemispherical	NA	NA	Ambient	1	2
LX-10	Slapper	NA	NA	Ambient	2	2
UFTATB	Slapper	4271-135M-02	1989	Ambient	3	2
UFTATB	Slapper	4271-135M-02	1991	Ambient	4	2
UFTATB	Slapper	4271-135M-02	1999	-20 °C	5	1
UFTATB	Slapper	4271-135M-02	1999	-54 °C	6	1
UFTATB	Slapper	00252135M	2000	-54 °C	7	1
UFTATB	Slapper	4271-135M-02	1987	Ambient	8	1
UFTATB	Slapper	4271-135M-02	1987	-54 °C	9	1

pressure values become less accurate later in time due to the diverging nature of the shock wave in the PMMA that the laser must travel through to the

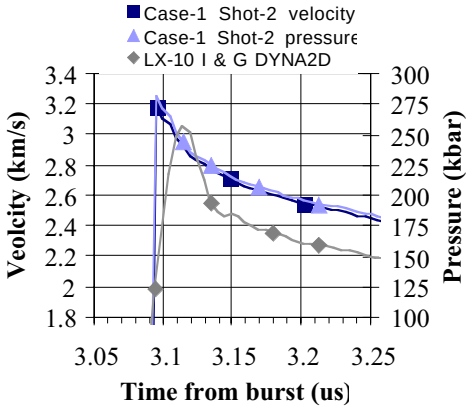

Figure 3. Comparison of velocity and pressure history for a typical LX-10 shot. The equivalent I & G DYNA2D model pressure profile is included for comparison.

aluminum surface. Figure 4 is a summary plot of breakout time for the LX-10, hemispherical detonator, shots. It can be seen in Fig. 4 that the breakout is quite uniform with the streak camera

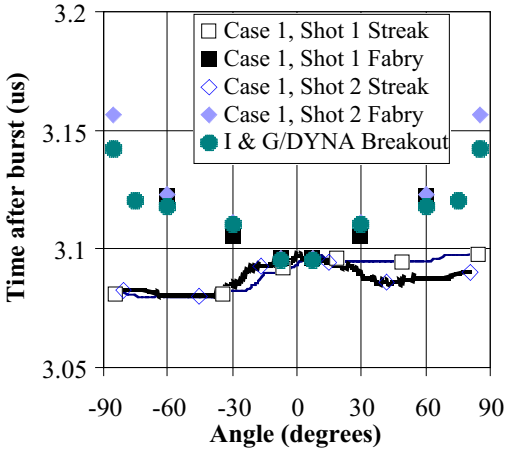

Figure 4. Breakout plot for Case 1 shots showing very flat breakout of the streak and somewhat greater curvature in the Fabry breakout. I & G DYNA2D model breakout times are included for comparison.

record showing flatness to within 20 ns. Figure 4 indicates that the breakout curvature around the booster indicated by the streak camera isn't totally consistent with the curvature indicated by the Fabry-Perot. The discrepancy is over 60 ns at some points with Fabry-Perot indicating the greater curvature. Note that the model agrees with the Fabry-Perot data. LX-10 is a relatively fast reacting explosive, which is modeled as releasing 90% of its energy in 20 - 30 ns and the remaining 10% over the 100 ns. If the LX-10 was an "ideal" explosive with infinitely fast reactions, the detonation wave in Fig. 4 would arrive at all 5 angles at the same time. The finite thickness of the LX-10 reaction zone causes the arrival time at 85˚ to be approximately 60 ns later than at 7˚ in both the experimental and calculated Fabry Perot records.

The discrepancy between the streak and Fabry-Perot timing has not been fully resolved. However, note that the velocity records were taken azimuthally 90° from the streak record; the discrepancy may be due to azimuthal nonuniformity in breakout. Timing discrepancies in the diagnostic system were considered, but ruled out. Figure 5 shows the effect of initiating LX-10 over a finite

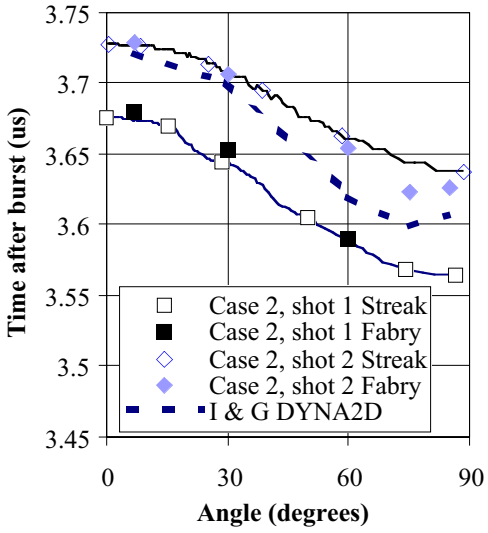

Figure 5. Breakout plot for case 2 shots. Note the breakout indicated by the I & G DYNA2D model which shows good agreement.

region using a two-stage slapper detonator. The experimental and calculated arrival times both differ by about 120 ns between 60˚ (earliest) and 7˚ (latest). The first arrival at 60˚ is a direct result of the finite diameter of the slapper flyer plate. The time difference resulting from geometry path differences would be 310 ns if the flyer were flat when it hit the booster. The record indicates that the spread of times from pole to equator is about 120 ns, indicating that there are other mechanisms at work. Other work has confirmed that the flyer is

not flat when it impacts the booster. Figure 6 is a plot of peak, or initial, pressure in the PMMA as the shock wave transitions the interface. The peak pressure with the slapper detonator is consistently higher than with the hemispherical detonator. Note a significant dip at 60° from the pole for the slapper detonator case. It can also be seen from Fig. 6 that there is scatter in the data and that the model predicts a somewhat lower peak pressure for both the hemispherical and slapper detonator initiated shots. These shots will probably not be repeated to improve data scatter.

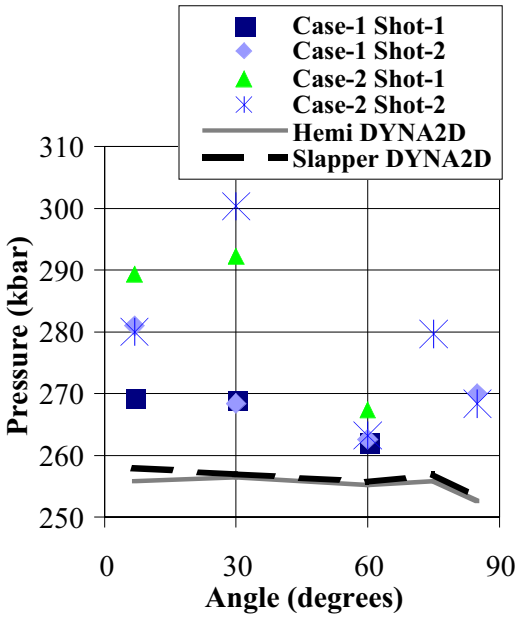

Figure 6. Plot of peak pressure for the LX-10 boosters. Case-1 is hemi-det. Case-2 is slapper det. I & G DYNA2D model results are

Figure 7 shows a summary of average breakout times for the experiments done at ambient temperature with *UFTATB* boosters. Note that the streak agrees very well with historical data, but that the average Fabry-Perot breakout appears to be shifted about 70 ns in time. While we believe that this is probably instrumentation error, the difference is variable and doesn't appear to be a systematic error. It is still under investigation. Also note from Fig. 7 that I & G DYNA2D model breakout times agree well with the Fabry-Perot data. The reaction rates used were G1 = 2200, G2 = 60. Figure 8 is a plot of breakout as seen by the Fabry-Perot for all of the *UFTATB* shots in this investigation, while Figure 9 is a plot of the peak pressure for the same shots. Figure 8 shows that the breakout time is quite consistent for all cases at the pole but slows near the equator as the temperature is reduced. This is consistent with historical data and with the model. The reaction rates used for cold *UFTATB*

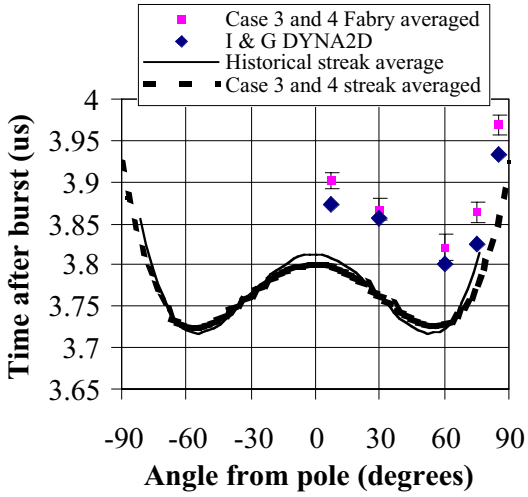

Figure 7. Comparison of breakout time indicated by streak and Fabry for ambient shots. Historical data is included to show agreement.

(G1 = 1575, G2 = 43) were reduced from the ambient temperature *UFTATB* rates by

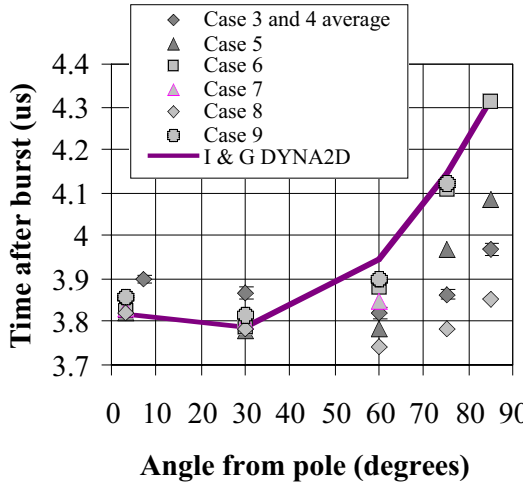

Figure 8. Plot of breakout time indicated by Fabry-Perot for all *UFTATB* cases in this investigation. The reduced-temperature I & G DYNA2D model results are included for comparison.

approximately the same percentage as that used for ambient and cold LX-17 and PBX 9502 in two companion papers.[5, 13] If the reaction rates were lowered slightly further to G1 = 1500, G2 = 41, cold *UFTATB* failed to shock initiate from the impact of the slapper flyer plate. Thus the cold *UFTATB* is

barely initiated by the flyer and is still building to full detonation when the wave strikes the PMMA

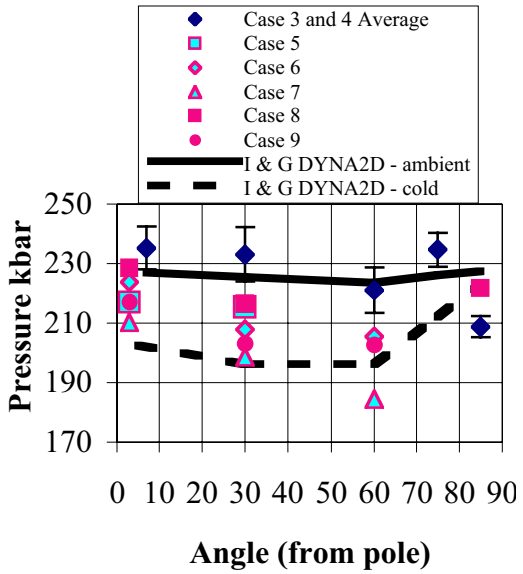

Figure 9. Comparison of peak pressure for all *UFTATB* shots. The I & G DYNA2D model results are included for comparison.

window. Spherically diverging waves in TATB-based explosives have long been known to require several centimeters of run distance to develop full steady state detonation conditions[8]. It can also be seen from Fig. 8 that the results from the oldest boosters are consistent with all other shots, indicating no adverse aging effects. Figure 9 shows that the peak pressure is consistent within about 10% for all conditions except Case 7, which shows a low pressure at the pole with a downward trend toward the equator. This shot will be repeated and will be investigated further if the behavior is repeatable. It can also be seen from Fig. 9 that the pressures predicted by the I & G DYNA2D model were generally consistent with experiment, but failed to predict a small "hump" in the pressure near the equator. This hump was consistent throughout the experimental shots. There is speculation that this pressure behavior might be due to density inhomogeneities in the boosters. Further study will be required to prove the hypothesis. The peak pressure is also consistent with detonation pressure in *TATB* determined by other means.

JWL++ Results

An X-ray tomograph showed density differences in the TATB part. These were erroneously thought initially to be several percent- a value that was later revised downward. This led us to construct multiple-region densities, as shown in Figure 10, which was run with JWL++. Each density region had a different JWL with a different

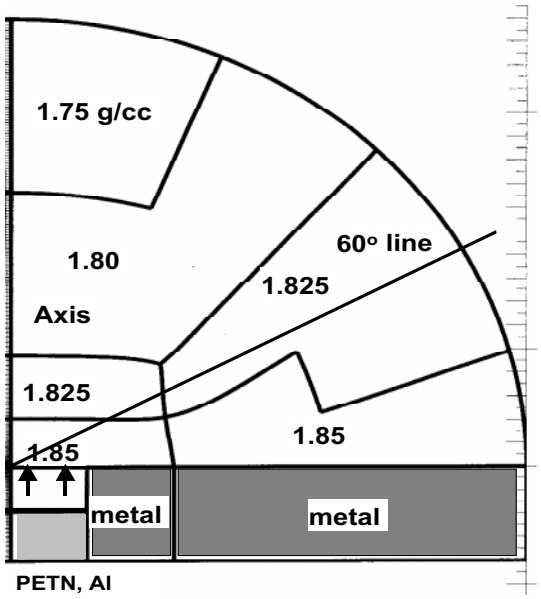

Figure 10. Schematic of the hemisphere with variable density sections, metal backing and PETN driving the flyer. The density variations used in this case are greater than those that we now believe exist.

resulting detonation velocity. The results are shown in Figure 11. Here, program burn clearly predicts the behavior badly, showing that the variable rate in Reactive Flow is necessary. The program burn was a ray-trace model, which reaches the back edge first because the outer edge of the slapper is closer to it. Both JWL++ runs get the minimum in the right place and are close to the data. Because the data splits the runs, this suggests that variable density could be a factor in this problem. We found that the booster is not a simple problem and reproducing the breakout in the code appears to be a combination of several things.

1) The slapper detonator breaks the spherical symmetry with a far end that extends toward the 60° surface. We began with all-radial zones but this is difficult to use, partly because of the tiny zones near the origin and partly because the sideways propagation of the detonation is too small. Various adjustments were made until we turned to the reduced connectivity mesh which appears to best describe the geometry. The three-region point can have advection problems and the 45° line can cause refraction.

2) The metal containment on the flat face is essential or the explosive will blow backward, thereby slowing down all the sideways burn. The metal speeds up the sideways propagation.

3) The time-dependent burn in the code is necessary to slow down the sideways propagation.

4) The detonation must be started promptly, which means turning it on quickly at the outer edges of the flyer. If it turns on too slowly, the sideways propagation will be too slow. The best results were obtained by modeling the actual PETN and flyer. Using other code initiation schemes such as node velocity are possible but the calibration appears difficult.

5) The variable density makes a difference because the detonation velocity scales with about the 2/3rds power of the density with a higher density path lying in the direction of 60^{o}.

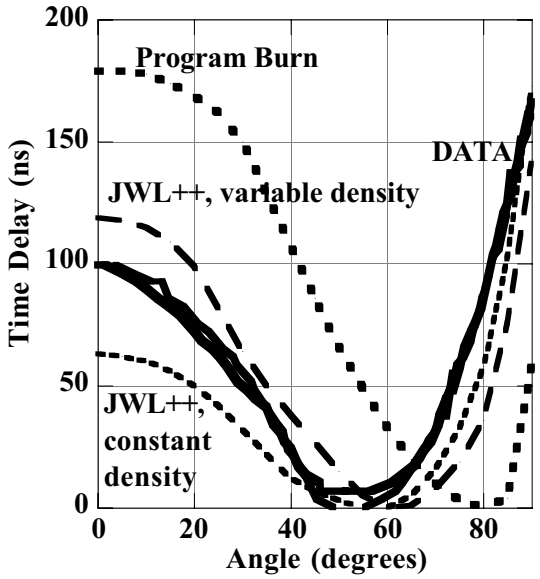

Figure 11. Comparison of code runs with the experimental data shown in Fig. 6. The light dashed lines are single density; the light full lines are variable density.

The first four issues all directly affect the sideways propagation and it is the balance of the four that makes the result occur. It is easy to set the code so that the leading point of the detonation front runs at the extremes, either down the axis or to outer edge. . This means that the code solution will not be unique and there will be many ways to adjust it.

REFERENCES

1. C. F. McMillan, D. R. Goosman, N.L. Parker, L.L. Steinmetz, H. H. Chau, T. Huen, R. K. Whipkey, and S. J. Perry, "Velocimetry of Fast Surfaces Using Fabry-Perot Interferometry," Rev. Sci. Instrum., V59, pp. 1-20, January 1988.

2. L.M. Barker and R. E. Hollenbach, "Shock-wave Studies of PMMA, Fused Silica, and Sapphire," Journal of Applied Physics, V41, pp. 4208-4226, September 1970.

3. J. Wackerle, H.L. Stacy and J.C. Dallman, "Refractive Index Effects for Shocked Windows in Interface Velocimetry," SPIE Vol. 832 High Speed Photography, Videography, and Photonics, pp. 72-82, 1987.

4. S. P. Marsh, editor, LASL Shock Hugoniot Data, University of California Press.

5. Tarver, C. M. and McGuire, E. M., "Reactive Flow Modeling of the Interaction of TATB Detonation Waves with Inert Materials," paper presented at this Symposium.

6. Tarver, C. M., Hallquist, J. O., and Erickson, L. M., Eighth Symposium (International) on Detonation, Naval Surface Weapons Center NSWC 86-194, Albuquerque, NM, 1985, p. 951.

7. Urtiew, P. A., Erickson, L. M., Aldis, D. F., and Tarver, C. M., Ninth Symposium (International) on Detonation, Office of the Chief of Naval Research OCNR 113291-7, Portland, OR, 1989, p. 112.

8. Bahl, K., Bloom, G., Erickson, L., Lee, R., Tarver, C., Von Holle, W., and Weingart, R., Eighth Symposium (International) on Detonation, Naval Surface Weapons Center NSWC MP 86-194, Albuquerque, NM, 1985, p. 1045.

9. Urtiew, P. A., Cook, T. M., Maienschein, J. L., and Tarver, C. M., Tenth International Detonation Symposium, Office of Naval Research, ONR 33395-12, Boston, MA, 1993, p. 139.

10. Urtiew, P. A., Tarver, C. M., Maienschein, J. L., and Tao, W. C., Combustion and Flame 105, 43 (1996).

11. Tarver, C. M., Propellants, Explosives and Pyrotechnics 15,132 (1990).

12. Urtiew, P.A., Tarver, C. M., Forbes, J. W., and Garcia, F., Shock Compression of Condensed Matter-1997, S. C. Schmidt, D. P. Dandekar, J. W. Forbes, eds., AIP Conference Proceedings 429, Woodbury, NY, 1998, p. 727.

13. Tran, T., Tarver, C., Maienschein, J., Lewis, P., Moss, M., Druce, R., Lee, R., and Roeske, F., "Characterization of Detonation Wave Propagation in LX-17 near the Critical Diameter," paper presented at this Symposium.

14. P. Clark Souers, Steve Anderson, Estella McGuire and Peter Vitello, "JWL++: A Simple Reactive Flow Code Package for Detonation," Propellants, Explosives, Pyrotechnics, 25, 54-58 (2000).

15. P. Clark Souers, Steve Anderson, Estella McGuire, Michael J. Murphy, and Peter Vitello, "Reactive Flow and the Size Effect," Propellants, Explosives, Pyrotechnics, 26, 26-32 (2001).